JMEPEG (2016) 25:656–667
DOI: 10.1007/s11665-015-1868-4


1059-9495/$19.00

# Laser Cladding of Composite Bioceramic Coatings on Titanium Alloy

*Xiang Xu, Jiege Han, Chunming Wang, and Anguo Huang*

*(Submitted June 15, 2015; in revised form December 12, 2015; published online January 6, 2016)*

**In this study, silicon nitride ($Si_3N_4$) and calcium phosphate tribasic (TCP) composite bioceramic coatings were fabricated on a Ti6Al4V (TC4) alloy using Nd:YAG pulsed laser, $CO_2$ CW laser, and Semiconductor CW laser. The surface morphology, cross-sectional microstructure, mechanical properties, and biological behavior were carefully investigated. These investigations were conducted employing scanning electron microscope, energy-dispersive x-ray spectroscopy, and other methodologies. The results showed that both $Si_3N_4$ and $Si_3N_4$/TCP composite coatings were able to form a compact bonding interface between the coating and the substrate by using appropriate laser parameters. The coating layers were dense, demonstrating a good surface appearance. The bioceramic coatings produced by laser cladding have good mechanical properties. Compared with that of the bulk material, microhardness of composite ceramic coatings on the surface significantly increased. In addition, good biological activity could be obtained by adding TCP into the composite coating.**

**Keywords** ceramic coating, laser cladding, prosthesis material, $Si_3N_4$, TCP

## 1. Introduction

Titanium alloys have broad applications in areas such as aerospace, marine, chemical industry, and biomedicine. Among them, Ti6Al4V (TC4) alloy has been widely used for an orthopedic implant material due to its superior properties including high mechanical properties, excellent corrosion resistance, and good biocompatibility (Ref 1). Surface treatments of titanium alloys are generally used to achieve superior surface finish and property. For a Ti-based medical implant, the surface needs to be tailored into a specific micro texture to enhance the adhesion with cells and bones (Ref 2).

Surface treatment via laser is an emerging technique to modify the surface properties of metals and their alloys (Ref 3, 4). Laser engineering net shaping (LENS)™ (Ref 5, 6), selective laser sintering, and selective laser melting (Ref 7-9) have shown significant advantages on structure preparation and surface engineering in biological research field. Laser cladding, as a competitive technique in surface preparation, is applied to fabricate coatings with dense microstructure and strong metallurgical bonding with the substrates. Recently, laser cladding has already been used in producing coatings on Titanium alloys for biomedical applications. However, it is a challenging task to obtain functional coatings with high wear resistance, high fracture toughness, and good biocompatibility. Current researches are mainly focused on the optimization of process parameters, and cladding materials to achieve desired coating properties (Ref 10).

Different lasers can be utilized for laser cladding in respect of particular applications. Nd:YAG laser is widely used in laser cladding due to its good absorptivity and machining precision. The $CO_2$ laser is suitable for laser cladding with high power, but its large spot size sacrifices the machining accuracy (Ref 11, 12). However, semiconductor laser can provide a relatively stable machining process and high quality of the machined surface due to its short wavelength, high absorption rate, and photoelectric transformation (Ref 13).

Silicon nitride ($Si_3N_4$) has been considered to be a potential candidate for clinical applications since it is a non-cytotoxic material and has satisfactory fracture toughness, high wear resistance, and low friction coefficient (Ref 14-17). In addition, calcium phosphate tribasic (TCP) is another promising material for bone reconstruction and remodeling. The bioresorbability of TCP encourages fast bone growth and facilitates integration with bone tissue as it resorbs (Ref 18, 19).

Several researches (Ref 20, 21) have been conducted to investigate the effect of various material combinations as surface modification materials on metal substrates by laser processing. However, few researches have focused on the enhancements of mechanical properties and biological activities of metal substrates, especially by means of different lasers. In this study, $Si_3N_4$ and TCP composite bioceramic coatings on TC4 alloy were fabricated using Nd:YAG pulsed laser, $CO_2$ CW laser, and Semiconductor CW laser. The objectives in this study are to fabricate appropriate composite ceramic coatings on the TC4 substrates through laser cladding and study the effect of process parameters on the surface morphologies and performances of coated bioceramics. In addition, the relationship between the surface integrity and biological performance of coated bioceramics was explored under different process parameters.

**Xiang Xu, Jiege Han, Chunming Wang,** and **Anguo Huang**, State Key Laboratory of Material Forming and Mould & Die Designing, School of Materials Science and Engineering, Huazhong University of Science and Technology, Wuhan 430074 Hubei, China. Contact e-mails: 413666436@qq.com, czxuxiang@sina.com, m15927496628@163.com, cmwang@mail.hust.edu.cn and huang-anguo@hust.edu.cn.

## 2. Experimental Procedure

### 2.1 Experimental Set Up

Figure 1 shows the three types of laser for the experiments. The Nd:YAG laser (Fig. 1a) is made by HGLASER and has a power of 500 W with a circular light spot. The second one is a HGL-HL-7000 continuous wave $CO_2$ laser (Fig. 1b) made by HGLASER with a rectangular broadband flare. The semiconductor laser (Fig. 1c) is made by DILAS Diodenlaser GmbH and has a power of 3000 W with a rectangular light spot.

### 2.2 Materials Selection

In this study, three groups of $Si_3N_4$ and TCP powders were used as coating materials, as shown in Table 1. A high percentage of $Si_3N_4$ powder was chosen as the basic component of the ceramic powder to ensure a stable coating surface. Different ratio TCP powders were added to study its effects to the bioactivity of the coating. The coating powder of each sample was laid on the top of a commercially TC4 substrate (6-mm thickness) by binders [0.5% polyvinyl alcohol (PVA) solution]. Since the property of the ceramic coating is closely dependent on its thickness, the layout of the ceramic powder is very important. Each group of coating powders was mixed using a planetary ball mill. Air compressor and F-75 spray gun were used to preset ceramic powders onto the substrate until the thickness of the coating is up to 100 μm.

### 2.3 Processing and Characterization

Laser cladding experiments were made relatively on each samples. In order to form the best cladding surface morphology, different process parameters were applied due to different laser characteristics. Energy input is thought to be the most important factor which determines the heat input during laser cladding. In this study, different energy inputs were selected through different parameters of lasers to find the effect on laser cladding. Energy inputs of each parameter were compared among different lasers which were calculated according to the following equations:

$$\mathrm{HI\,(J/mm)} = \eta \frac{I(\mathrm{A})U(\mathrm{V})W(\mathrm{s})f(\mathrm{HZ})}{V_s(\mathrm{mm/s})}\ (\text{in Group 1})$$

$$\mathrm{HI\,(J/mm)} = \eta \frac{P(\mathrm{W})}{V_s(\mathrm{mm/s})}\ (\text{in Group } 2 \sim 3),$$

where HI is the energy input, $\eta$ the coefficient of laser cladding efficiency, $I$ the current intensity, $U$ the voltage, $W$ the pulse width of the laser, $f$ the frequency of the laser, $P$ the power of laser cladding, and $V_s$ the speed of laser cladding.

Table 2 shows the machining conditions of the three lasers.

After laser cladding, all samples were firstly cross-sectioned, and then ground by sand paper up to 2000 grit and polished with a diamond polishing paste. Later on, samples were further chemically rinsed for 15 s in the solution of hydrofluoric acid, hydrochloric, nitric acid, and distilled water (volume ratio of 1:1.5:2.5:95). Then, the cross-sectional microstructure of each

**Table 1 Coating powder compositions**

| Group | $Si_3N_4$ (wt.%) | TCP (wt.%) |
|---|---|---|
| A | 100 | 0 |
| B | 90 | 10 |
| C | 80 | 20 |

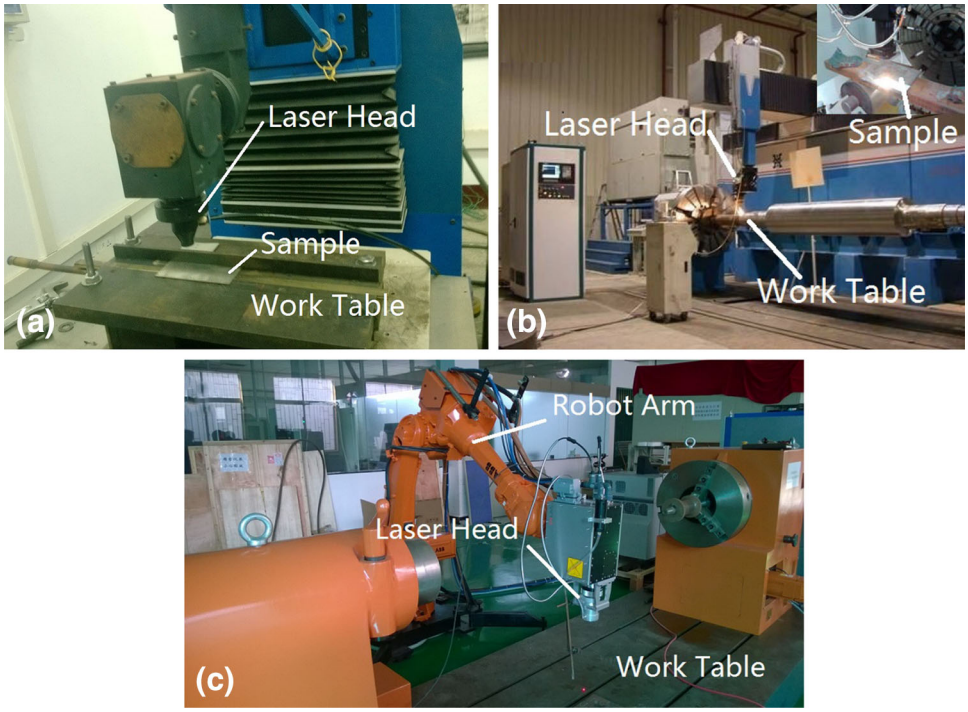


**Fig. 1** Lasers (a: Nd:YAG laser; b: $CO_2$ laser; c: Semiconductor laser)

**Table 2 Laser cladding parameters**

| Group | Laser | Number | Coating compositions | Fixed parameters | Experiment parameters | Energy input/J mm$^{-1}$ |
|---|---|---|---|---|---|---|
| 1 | Nd:YAG laser | A1-1 | $Si_3N_4$ | Spot diameter: $\varphi = 0.8$ mm; Pulse width: $W = 2.0$ ms; Supply current: $I = 120$ A; Percent conversion: $\eta = 3\%$; | Laser frequency: 12HZ; Scan speed: 80 mm/min; | 24.62 |
| | | A1-2 | | | Laser frequency: 12HZ; Scan speed: 100 mm/min; | 19.70 |
| | | A1-3 | | | Laser frequency: 12HZ; Scan speed: 120 mm/min; | 16.42 |
| | | A1-4 | | | Laser frequency: 11HZ; Scan speed: 100 mm/min; | 18.06 |
| | | A1-5 | | | Laser frequency: 13HZ; Scan speed: 100 mm/min; | 21.34 |
| | | B1-1 | $Si_3N_4$ + 10%TCP | | Laser frequency: 12HZ; Scan speed: 45 mm/min; | 43.78 |
| | | B1-2 | | | Laser frequency: 12HZ; Scan speed: 80 mm/min; | 24.62 |
| | | B1-3 | | | Laser frequency: 12HZ; Scan speed: 100 mm/min; | 19.70 |
| | | B1-4 | | | Laser frequency: 11HZ; Scan speed: 100 mm/min; | 18.06 |
| | | B1-5 | | | Laser frequency: 13HZ; Scan speed: 100 mm/min; | 21.34 |
| | | C1-1 | $Si_3N_4$ + 20%TCP | | Laser frequency: 12HZ; Scan speed: 80 mm/min; | 24.62 |
| | | C1-2 | | | Laser frequency: 12HZ; Scan speed: 100 mm/min; | 19.70 |
| | | C1-3 | | | Laser frequency: 12HZ; Scan speed: 120 mm/min; | 16.42 |
| | | C1-4 | | | Laser frequency: 11HZ; Scan speed: 100 mm/min; | 18.06 |
| | | C1-5 | | | Laser frequency: 13HZ; Scan speed: 100 mm/min; | 21.34 |
| 2 | $CO_2$ laser | C2-1 | $Si_3N_4$ + 20%TCP | Spot size: 15mm×2mm; Percent conversion: $\eta = 10\%$; | Laser power: 1000 W; Scan speed: 200 mm/min | 30 |
| | | C2-2 | | | Laser power: 1120 W; Scan speed: 200 mm/min; | 33.6 |
| | | C2-3 | | | Laser power: 1150 W; Scan speed: 200 mm/min; | 34.5 |
| | | C2-4 | | | Laser power: 1120 W; Scan speed: 180 mm/min; | 37.3 |
| | | C2-5 | | | Laser power: 1120 W; Scan speed: 220 mm/min; | 30.5 |
| 3 | Semiconductor laser | A3-1 | $Si_3N_4$ | Spot size: 3 mm × 3 mm; Percent conversion: $\eta = 50\%$; | Laser power: 400 W; Scan speed: 10 mm/s | 20 |
| | | A3-2 | | | Laser power: 500 W; Scan speed: 10 mm/s; | 25 |
| | | A3-3 | | | Laser power: 400 W; Scan speed: 5 mm/s; | 40 |
| | | B3-1 | $Si_3N_4$ + 10%TCP | | Laser power: 500 W; Scan speed: 10 mm/s; | 25 |
| | | B3-2 | | | Laser power: 400 W; Scan speed: 10 mm/s; | 20 |
| | | B3-3 | | | Laser power: 500 W; Scan speed: 20 mm/s; | 12.5 |
| | | C3-1 | $Si_3N_4$ + 20%TCP | | Laser power: 500 W; Scan speed: 10 mm/s; | 25 |
| | | C3-2 | | | Laser power: 600 W; Scan speed: 10 mm/s; | 30 |
| | | C3-3 | | | Laser power: 400 W; Scan speed: 5 mm/s; | 40 |

sample was examined by optical microscope (VHX-1000C) and field emission scanning electron microscope (FE-SEM) (JSM-7600F, JEOL, Tokyo, Japan). Energy-dispersive spectroscopy (EDS) was also used for qualitative chemical analysis of the coated bioceramics. Vickers microhardness measurements (HX-1000) were made on the composite ceramic coating samples using the load of 1 kg for 15 s.

The bone-bonding ability of the coating is usually evaluated by the formation of apatite on its surface in a simulated body fluid (SBF), which has similar ion concentrations with human blood plasma. As shown in Table 3 (Ref 22), different reagents and distilled water are used to prepare the SBF-simulated solution. The in vitro bioactivities of the coatings above were analyzed in SBF. Samples made of different

coatings were immersed in the prepared SBF solutions under static conditions inside a biological thermostat at 37 °C for different weeks. After exposure, samples were washed with distilled water and then dried at 50 °C for 24 h. After these, both SEM and EDS were used to evaluate the formation of apatite-like composition, which is a useful indicator of in vivo bone bioactivity.

## 3. Results and Discussions

### 3.1 Microstructure of the Coatings

**3.1.1 Coating by Nd:YAG Laser.** A 500 W pulsed Nd-YAG laser system with a circular light spot was used in the first group to fabricate the composite ceramic coating. The spot size,

**Table 3 Amounts and weighing containers of reagents for preparing 1000 ml of SBF**

| Order | Reagent | Amount | Order | Reagent | Amount |
|---|---|---|---|---|---|
| 1 | NaCl | 8.035 g | 6 | 1.0 M-HCl | 39 ml |
| 2 | $NaHCO_3$ | 0.355 g | 7 | $CaCl_2$ | 0.292 g |
| 3 | KCl | 0.225 g | 8 | $Na_2SO_4$ | 0.072 g |
| 4 | $K_2HPO_4 \cdot 3H_2O$ | 0.231 g | 9 | Tris | 6.118 g |
| 5 | $MgCl_2 \cdot 6H_2O$ | 0.311 g | 10 | 1.0 M-HCl (bal) | 0-5 ml |

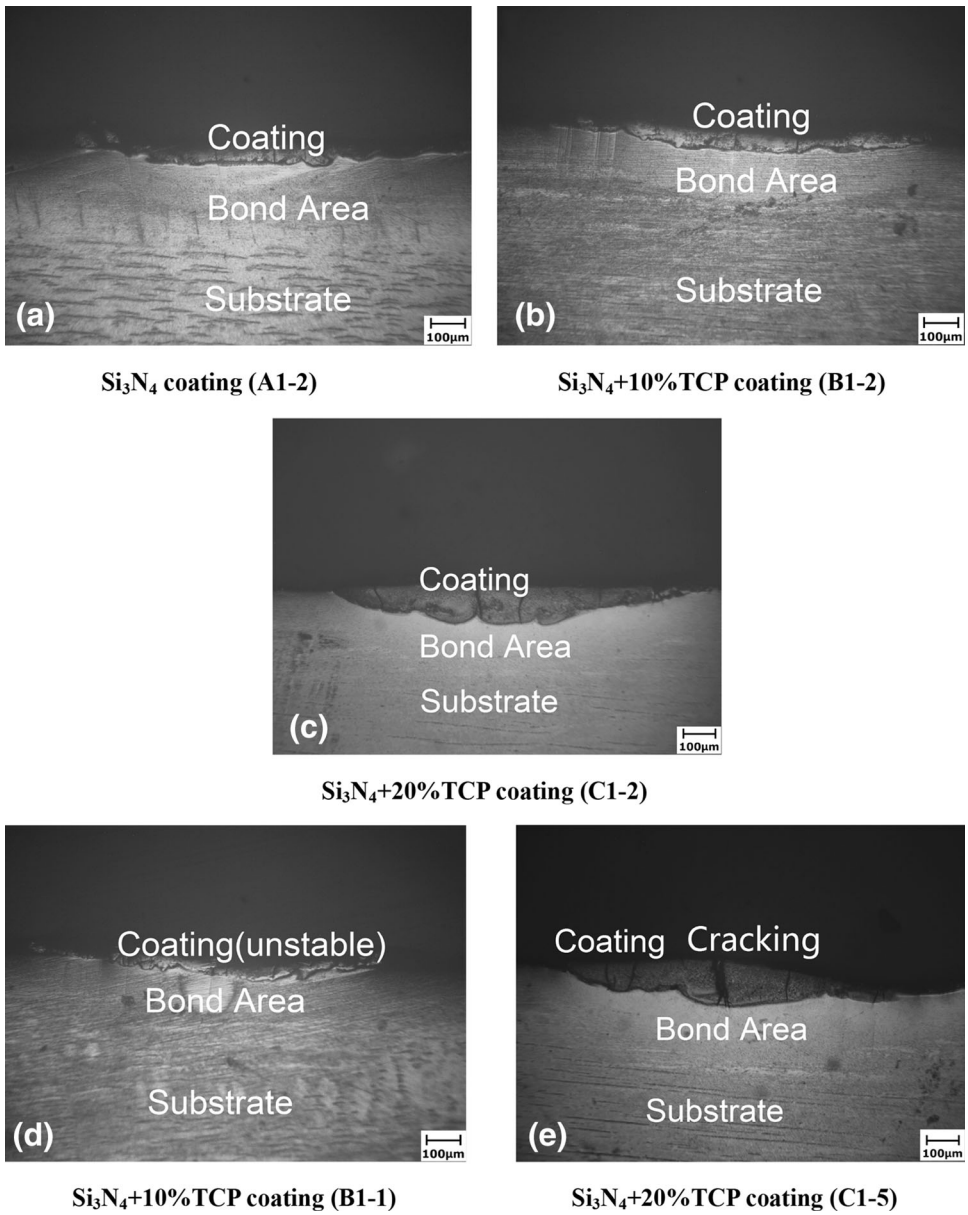


**$Si_3N_4$ coating (A1-2)**

**$Si_3N_4$+10%TCP coating (B1-2)**

**$Si_3N_4$+20%TCP coating (C1-2)**

**$Si_3N_4$+10%TCP coating (B1-1)**

**$Si_3N_4$+20%TCP coating (C1-5)**

**Fig. 2** OM micrographs of ceramic coating coatings on TC4 by pulsed Nd:YAG laser (×100) (a) $Si_3N_4$ coating (A1-2) (b) $Si_3N_4$ + 10%TCP coating (B1-2) (c)$Si_3N_4$ + 20%TCP coating (C1-2) (d) $Si_3N_4$ + 10%TCP coating (B1-1) (e) $Si_3N_4$ + 20%TCP coating (C1-5)

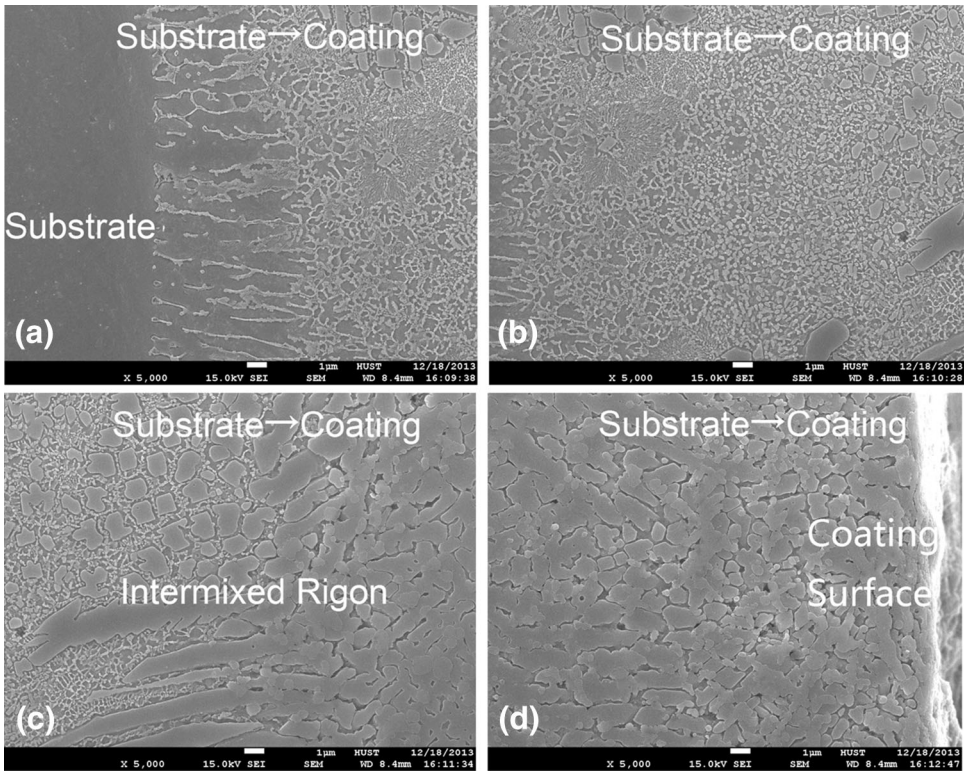


**Fig. 3** SEM micrographs of the $Si_3N_4$ + 10%TCP coating (B1-3) a-d showing the microstructure from substrate-coating interface to coating surface

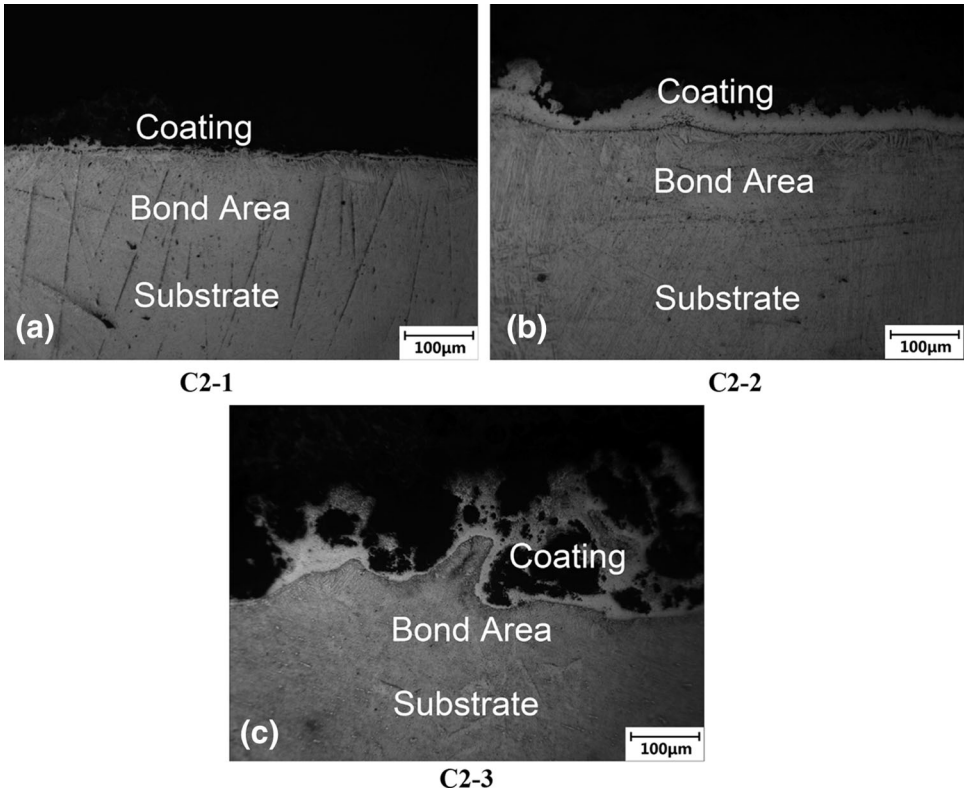


**Fig. 4** OM micrographs of $Si_3N_4$ +20%TCP coatings on TC4 by continuous wave $CO_2$ laser (×200) (a) C2-1 (b) C2-2 (c) C2-3

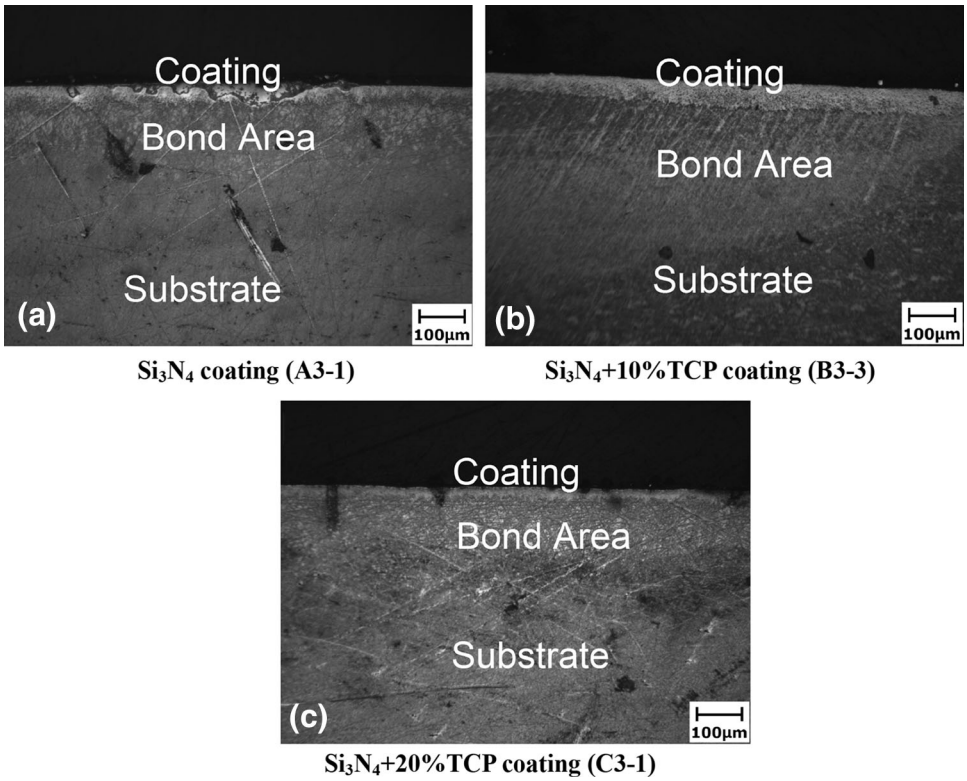


**$Si_3N_4$ coating (A3-1)** **$Si_3N_4$+10%TCP coating (B3-3)**

**$Si_3N_4$+20%TCP coating (C3-1)**

**Fig. 5** OM micrographs of ceramic coatings on TC4 by semiconductor laser (×100) (a) $Si_3N_4$ coating (A3-1) (b) $Si_3N_4$ + 10%TCP coating (B3-3) (c) $Si_3N_4$ + 20%TCP coating (C3-1)

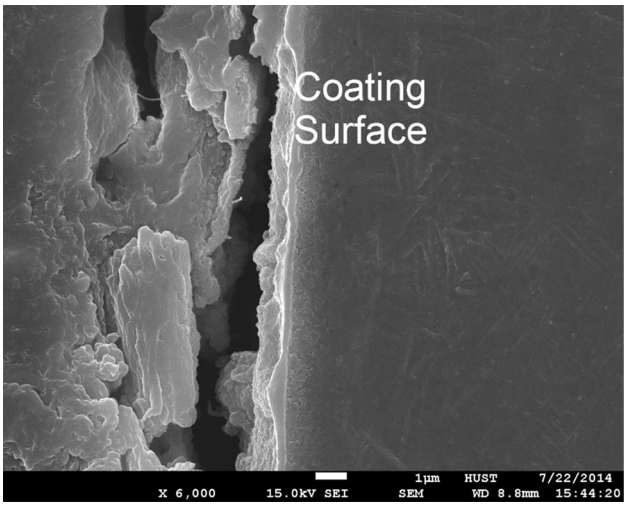


**Fig. 6** SEM micrographs of the $Si_3N_4$ + 10%TCP coating (B3-3)

pulse width, and supply current were fixed; as shown in Table 2, scan speed and laser frequency were changed to study their influences on the microstructure.

Figure 2a-c shows the optical microscope (OM) images of cross section of the coatings, which have different TCP contents but close appropriate laser cladding parameters (A1-2, B1-2, C1-2). The microstructures of the coating were well bonded with the substrates without any visible defects. However, the coating with higher power intensity in laser cladding was severely damaged, as shown in Fig. 2d (B1-1). It was believed that there should be a critical power intensity, above which the laser cladding coating would be damaged. When the laser power was increased or the scanning speed was decreased, non-uniform thickness and degraded ceramic coating quantity would be observed. In addition, the composition of the ceramic powders would also influence the surface integrity of the coating. Microcracks were found in the coating with higher TCP contents as shown in Fig. 2e (C1-5). This could be explained by the difference of melting temperatures among those materials. Since $Si_3N_4$ (&1850 °C) have a higher melting point than the TC4 substrate (1668 °C) when the melting point of TCP is only 1391 °C, the solidification range of the molten pool will widen during the solidification process. When the content of TCP in the composite ceramic coating is higher, earlier solidified TC4 and remaining TCP liquid membrane between the $Si_3N_4$ grains may split due to the restraint stress, which leads to cracking (Fig. 2e, C1-5) near the solidus (Ts). When the content of TCP in the composite ceramic coating is lower, the composite ceramic coating possesses a perfect compact structure since few TCP liquid film will fill the spaces between the $Si_3N_4$ and TC4 grains; as a result, no crack defects would be generated.

Typical microstructure of $Si_3N_4$ + 10%TCP composite ceramic coating sample (B1-3) is shown in Fig. 3. As shown in Fig. 3a, at the substrate-coating interface, the coating exhibited good metallurgical bonding with substrate layer, indicating strong bonding with the TC4 substrate. In addition, a compositional gradient of the coating and obvious intermixed region can be seen in Fig. 3a-c. Fully columnar crystal phases in the subsurface evolved to equiaxed crystal phase in the top surface.

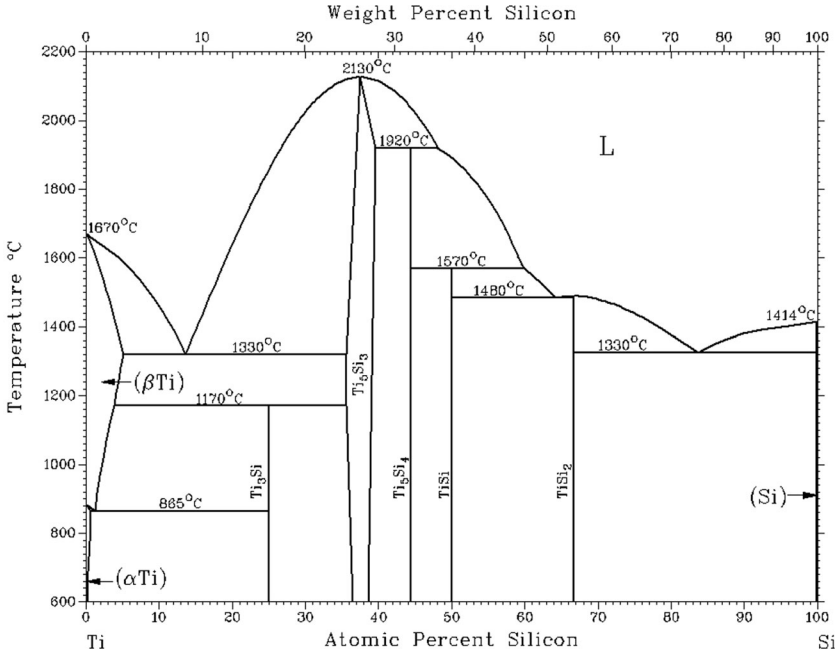


**Fig. 7** Ti-Si binary alloy phase diagram (Ref 23)

**Table 4 Comparison of the coatings manufactured by different lasers**

| Group | Laser | Laser rated power | Laser waveform | Surface topography | Stability | Efficiency |
|---|---|---|---|---|---|---|
| 1 | Nd:YAG laser | 500 W | Pulsed wave | Good | Good | Low |
| 2 | Crosscurrent $CO_2$ laser | 7000 W | Continues wave | Non-uniform | Poor | High |
| 3 | Semiconductor laser | 3000 W | Continues wave | Good | Good | Normal |

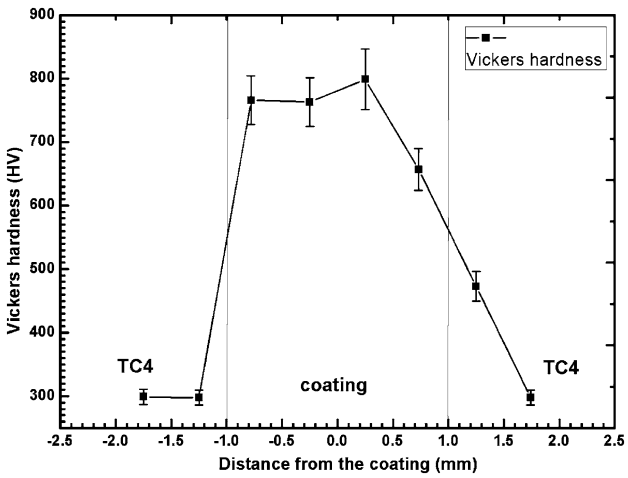


**Fig. 8** Hardness profile of coating fabricated by Nd:YAG laser surface

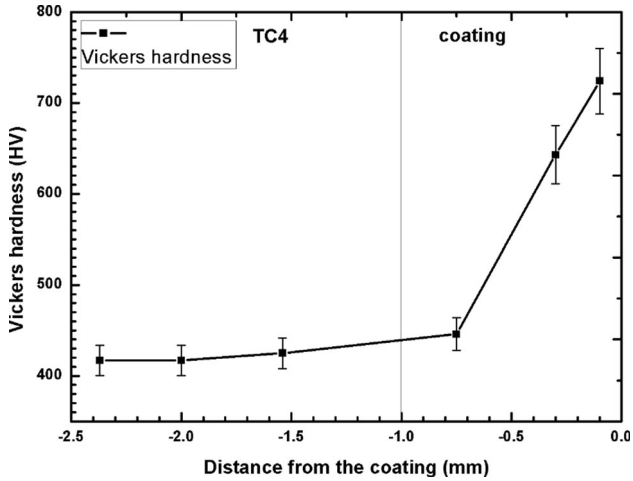


**Fig. 9** Hardness profile of coating fabricated by semiconductor laser surface

The microstructure near the coating surface is shown in Fig. 3d. $Si_3N_4$ grains with different grain sizes were observed, which may be result from different cooling rates. Smaller grains are likely to form near the top surface where a higher cooling rate was obtained.

### 3.2 Coating by $CO_2$ Laser

A HGL-HL-7000 continuous wave $CO_2$ laser system with a rectangular flare broadband was used in the second group to fabricate the composite ceramic coating. Table 2 shows the

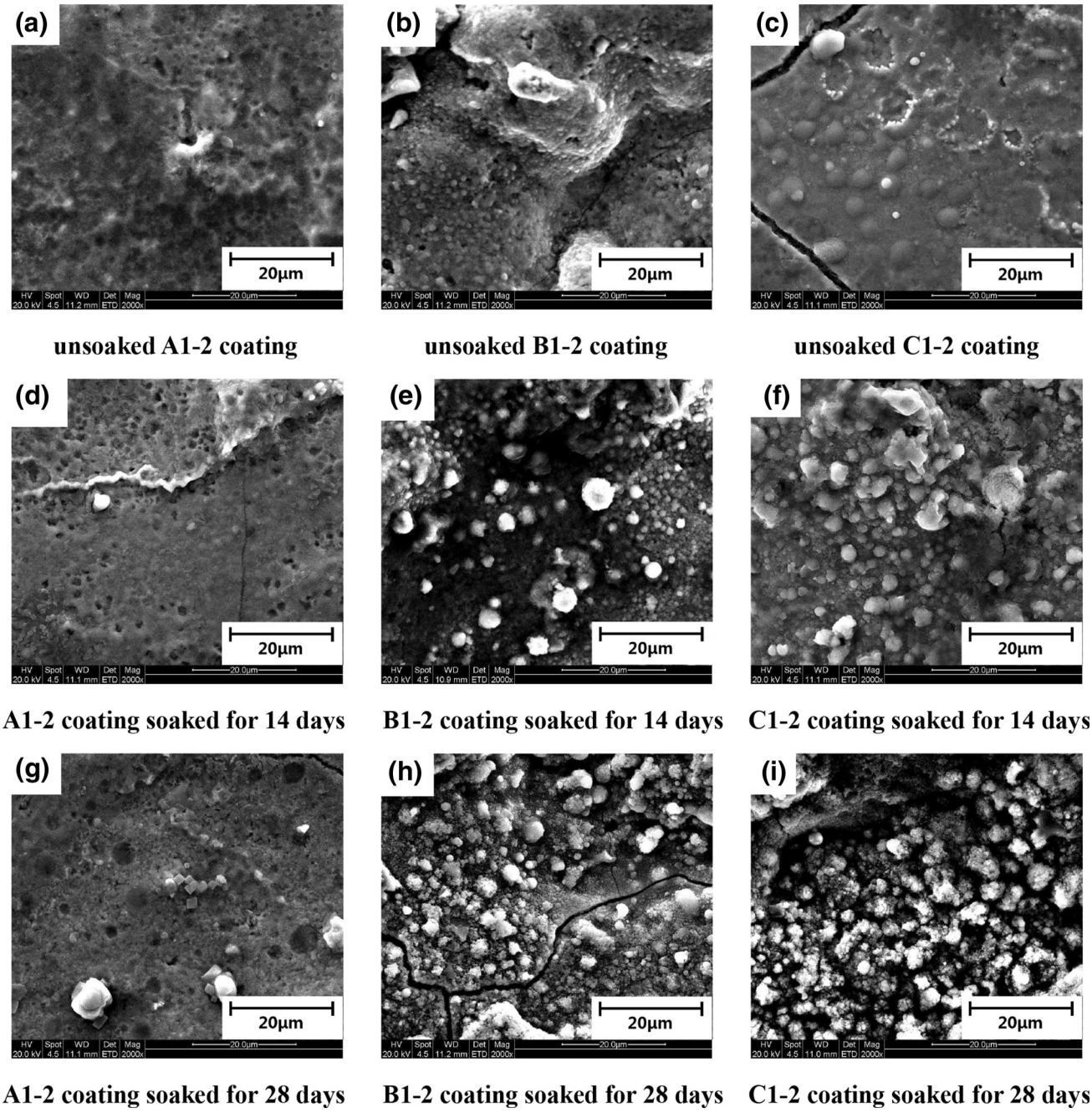


**Fig. 10** SEM analyses of the $Si_3N_4$ $Si_3N_4$ + 10%TCP, $Si_3N_4$ + 20%TCP coating surfaces after exposure in SBF unsoaked A1-2 coating (b) unsoaked B1-2 coating (c) unsoaked C1-2 coating (d) A1-2 coating soaked for 14 days (e) B1-2 coating soaked for 14 days (f) C1-2 coating soaked for 14 days (g) A1-2 coating soaked for 28 days (h) B1-2 coating soaked for 28 days (i) C1-2 coating soaked for 28 days

parameters of scan speed and laser power with a fixed rectangular spot size of 14 mm × 2 mm. Figure 4 shows the subsurface microstructure of $Si_3N_4$ + 20%TCP coating samples by three different laser cladding parameters (C2-1, C2-2, and C2-3). The coating thickness increased by about 50% when the laser power increased from 1000 to 1120 W. However, a further increased laser power (1150 W) resulted in a sporadic coating layer, instead of a thicker one (Fig. 4c). This was because excessively high laser power damaged the coating by decomposing the ceramic. By comparing the subsurface microstructure of the coated samples in different laser parameters, an optimized parameter (1120 W and 200 mm/min) was obtained which leaded to a stable and uniform composite ceramic coating.

**3.2.1 Coating by Semiconductor Laser.** A 3000 W semiconductor laser with a rectangular light spot was used in the third group to fabricate the composite ceramic coating. Table 2 shows the parameters of scan speed and laser power with a fixed rectangular spot size of 3 mm × 3 mm.

Figure 5a-c shows the subsurface microstructure of three laser cladding samples from different ceramic compositions (A3-1, B3-3, and C3-1). Superior bondings, few of cracks or fusion defects, could be seen in the optimized parameters. Compared with Fig. 3e, fewer microcracks were found in the

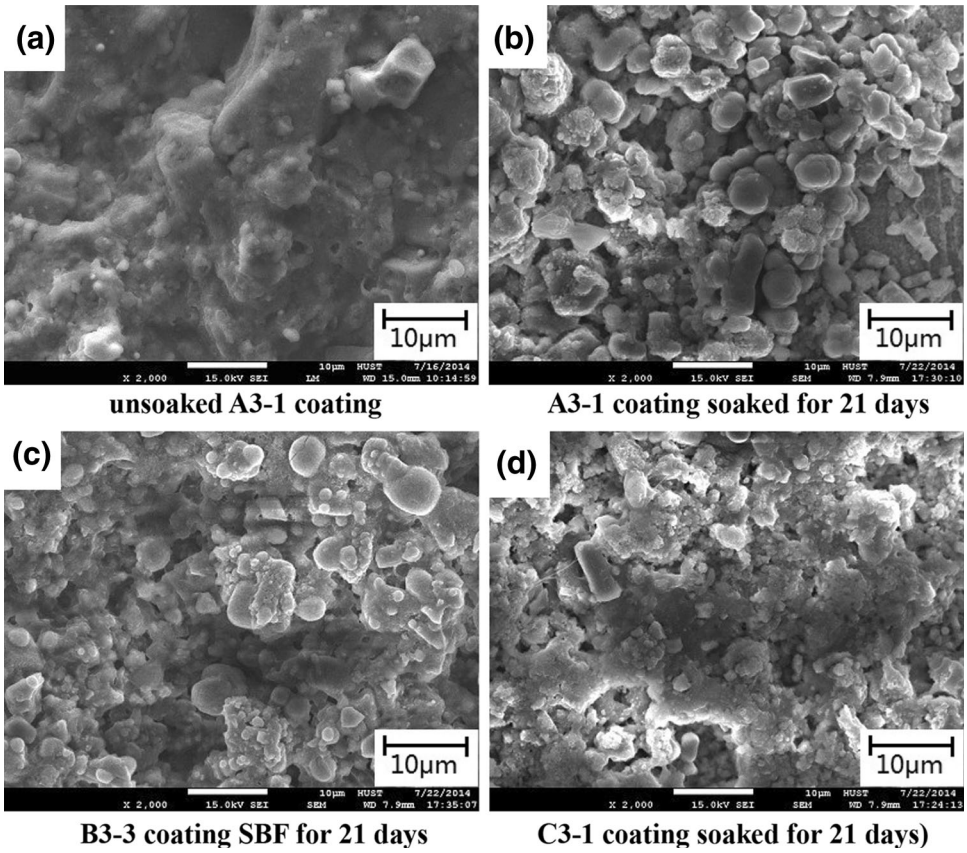


**Fig. 11** SEM analyses of the $Si_3N_4$, $Si_3N_4$ + 10%TCP, $Si_3N_4$ + 20%TCP coating surfaces after exposure in SBF (a) unsoaked A3-1 coating (b) A3-1 coating soaked for 21 days (c) B3-3 coating SBF for 21 days (d) C3-1 coating soaked for 21 days)

coating with higher TCP contents as shown in Fig. 5c (C3-1) because of different laser characteristics. The thickness of the coating ranged between 20 and 50 μm.

A higher magnification image of $Si_3N_4$ + 10%TCP coating was characterized by SEM (Fig. 6). Figure 6 shows a good forming appearance near the coating surface. Similar with the coating by Nd:YAG laser, equiaxed $Si_3N_4$ grains can be seen near the coating surface, diffusely distributed with TCP grains.

A simulated Ti-Si binary alloy phase diagram is shown in Fig. 7. A region containing eutectic crystal can be found when the temperature is above 1330 °C and the Si content is located at 20-35%. As in conjunction with Fig. 3 and 6, a eutectic structure can form between coating and substrate due to high energy of laser, which ensures a high bonding strength and stable transition structure from substrate to coating surface.

**3.2.2 Effect of Different Laser Systems on Ceramic Coatings.** The surface topography of an orthopedic implant can critically alter the cellular response at the tissue-implant interface (Ref 24). As shown in Table 3, three types of laser have been successfully applied to coat the TC4 subsurface with uniformly distributed $Si_3N_4$/TCP.

However, different surface topography, microstructures, and characteristics can be obtained by different lasers. Nd:YAG laser provides better cladding topography, but it is difficult to be used at a practical level due to the slow productivity and instability of the deposition process. The continuous wave $CO_2$ laser with spot size of 2 mm × 14 mm ensures the high productivity, but the bad formability and non-uniform surface finish. The semiconductor laser is able to provide a stable output power, and high photoelectric conversion rate which ensures the good coating surface morphology and fewer microdefects. Also, the 3 mm × 3 mm spot size ensures the high efficiency.

Ceramic coatings fabricated by Nd:YAG laser and semiconductor laser showed intermixed regions with gradient compositions. Pure TC4 can be found in the coating near the subsurface and full of $Si_3N_4$/TCP on the coating surface. The microstructures of the coatings evolved from columnar crystal phase to equiaxed crystal phase with the coating transiting from the substrate to the surface. In addition, the intermixed region by semiconductor laser was much thinner than the one by Nd:YAG laser.

As shown in Table 4, coatings fabricated by $CO_2$ laser in Group 2 showed a poor and less stable surface morphology which was undesirable, so samples in Group 2 have to be canceled in further performance tests.

### 3.3 Microhardness of the Coatings

Since surface mechanical properties of the coatings can be evaluated by the surface hardness, Vickers microhardness was measured to characterize the wear resistance of the composite ceramic coatings. The composite ceramic coating samples fabricated by Nd:YAG laser and Semiconductor laser were tested by HX-1000 microindenter.

**3.3.1 Microhardness by Nd:YAG Laser.** Three repeated measurements of Vicker's microhardness measurements (HX-1000) were performed on the transverse sections of the coating

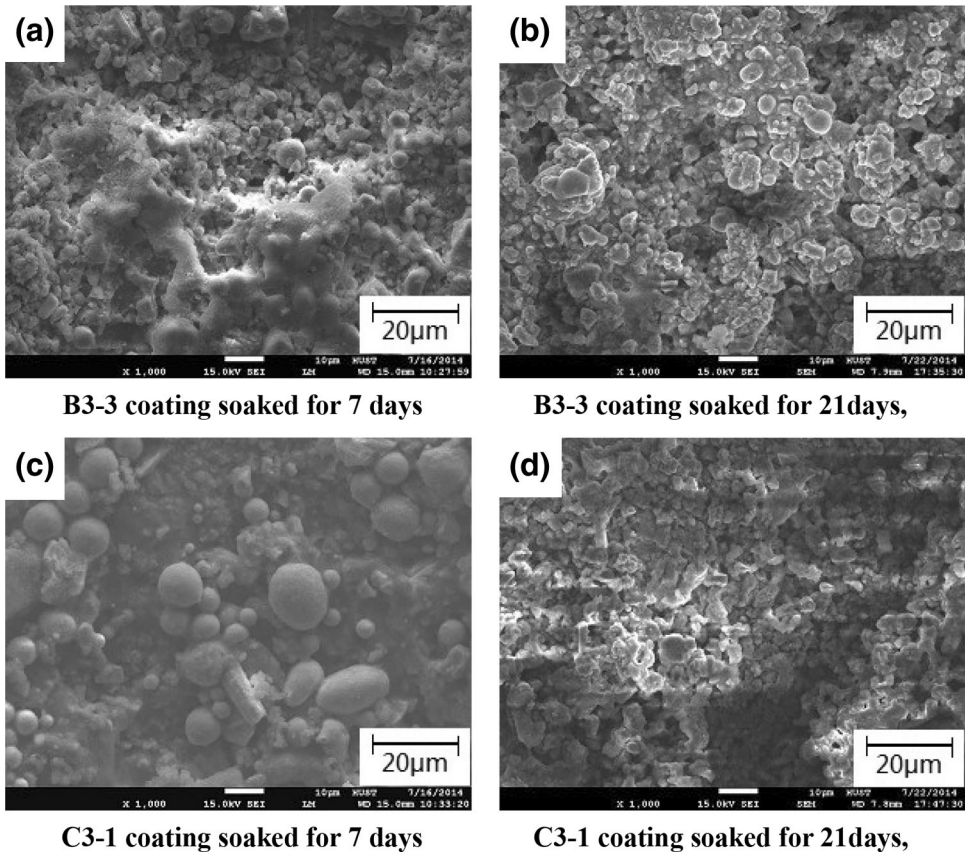


**Fig. 12** SEM analyses of the $Si_3N_4$ + 10%TCP, $Si_3N_4$ + 20%TCP coating surfaces after exposure in SBF (a) B3-3 coating soaked for 7 days (b) B3-3 coating soaked for 21 days, (c) C3-1 coating soaked for 7 days (d) C3-1 coating soaked for 21 days

fabricated by Nd:YAG laser. The average hardness profiles of three groups of sample C1-2 are shown in Fig. 8. The microhardness increased from 307 to 333 HV at the substrate to 760-856 HV in the coating. The asymmetry and fluctuation of hardness profiles are found in Fig. 8 due to the uneven distribution of ceramic components in certain areas. Compared with the substrate area, the microhardness of the coating area was largely increased because of the addition of ceramic components.

**3.3.2 Microhardness by Semiconductor Laser.** Figure 9 shows three repeated measurements of the Vicker's microhardness (HX-1000) on longitudinal section of the coating fabricated by semiconductor laser (sample C3-1). The microstructural variation across the coating thickness resulted in a gradual increase in hardness from the interface (420-430 HV) to the coating (542-701 HV). Because of the existence of ceramic components, the microhardness near the coating surface increases to 730-749 HV, almost twice harder than the substrate (410-420 HV).

### *3.4 Bioactivity of the Coatings*

**3.4.1 Bioactivity of the Coatings Fabricated by Nd:YAG Laser.** After laser cladding, samples were cleaned by acetone and distilled water before the bioactivity testing. Samples made of three different coatings (A1-2, B1-2, and C1-2) were immersed in the prepared SBF solutions (20 ml) for 14 and 28 days.

Figure 10 shows surface topography of different coatings (pure $Si_3N_4$ coating, $Si_3N_4$ + 10%TCP coating and $Si_3N_4$ + 20% TCP coating) after different soaking conditions. For the pure $Si_3N_4$ coating, microcracks and a trace of precipitates can be observed on the surface after immersing in SBF for 14 days (Fig. 10d). With the immersing time increasing to 28 days (Fig. 10g), larger precipitates as well as microcracks occurred on the surface. For the $Si_3N_4$ + 10%TCP coating, much more precipitates were found on the surface after immersing in SBF than those of pure $Si_3N_4$ coatings. As shown in Fig. 10e, several spherical grains formed on the surface after 14 days, and proportionally increased with immersing time (Fig. 10h). Microcracks could also be observed after immersing for 28 days. For the $Si_3N_4$ + 20%TCP coating, obvious microcracks were found after laser cladding due to the high-tensile residual stress, while the cracks were removed after immersing in SBF for 28 days (Fig. 10i). Similarly, more precipitates were formed on the surface by immersing for 28 days than that of 14 days (Fig. 10h).

**3.4.2 Bioactivity of the Coatings Fabricated by Semiconductor Laser in SBF.** Similarly with the coatings cladded by Nd:YAG laser, the samples fabricated by semiconductor laser were immersed in SBF solutions (20 ml) for 7 and 21 days. Figure 13b-d shows the SEM images of surface topography of coated samples after immersing in SBF for 21 days. Compared to the unsoaked sample (Fig. 11a), $Si_3N_4$/TCP coating surfaces were covered with different sizes of grains after immersing for 21 days. Unlike Fig. 10, no

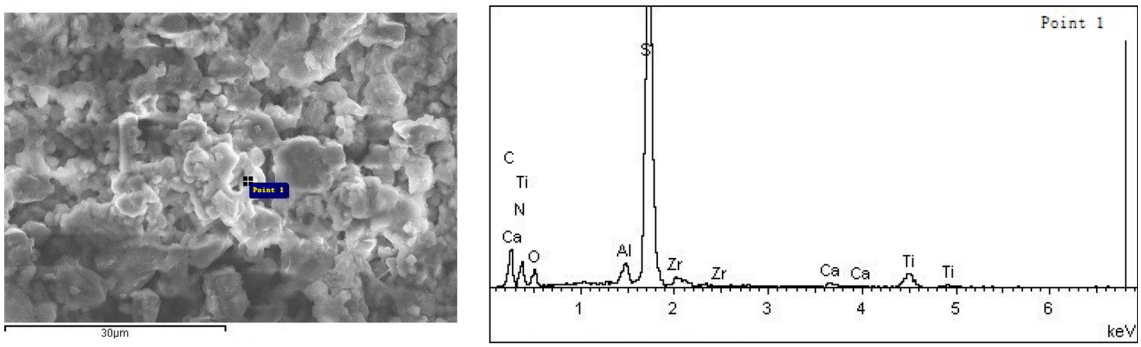


(a) unsoaked C3-1 coating

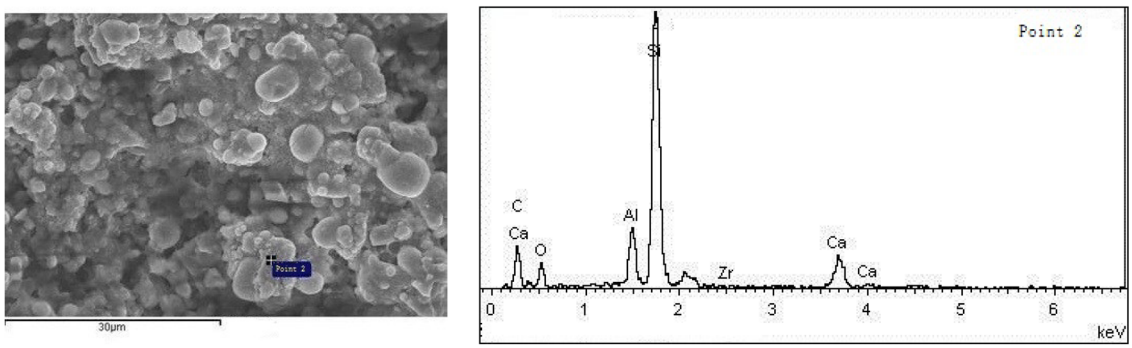


(b) C3-1 coating soaked in SBF for 21days

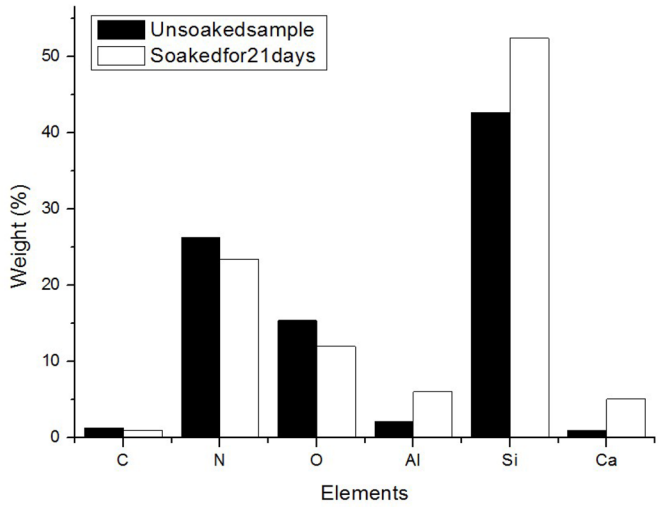


(c) Element distribution of different $Si_3N_4$+20%TCP samples after exposure in SBF

**Fig. 13** EDS analyses of $Si_3N_4$ + 20%TCP coating surfaces after exposure in SBF (a) unsoaked C3-1 coating (b) C3-1 coating soaked in SBF for 21 days (c) Element distribution of different $Si_3N_4$ + 20%TCP samples after exposure in SBF

microcrack is found in Fig. 11 because of the laser characteristic. In addition, a higher content of TCP in the coating resulted in a better formability of apatite-like composition as shown in Fig. 13c and d.

Figure 12 shows the surface topography of $Si_3N_4$ + 10%TCP, $Si_3N_4$ + 20%TCP samples soaked in SBF for 7 and 21 days, respectively. For the coating of $Si_3N_4$ + 10%TCP, more grains were found on the surface after immersing for 21 days (Fig. 12a) than that of 7 days (Fig. 12b). Also, the grains prefer to cluster with each other after a longer immersing time. Similar results could be observed in the coating of $Si_3N_4$ + 20%TCP.

EDS spectra of both unsoaked $Si_3N_4$ + 20%TCP coating sample and the soaked one are shown in Fig. 13. After immersing in the SBF for 21 days, the contents of elements with high atomic number (Al, Si, and Ca) increased, while those with low atomic number (C, N, and O) decreased. Since Ca and P are the most necessary elements for the formation of apatite, the increased Ca content partly indicated a good apatite-like compositions formability of the $Si_3N_4$ + 20%TCP sample. In further work, longer immersing time could be selected to find the obvious increase of P and Ca to further verify the apatite-forming ability of the composite coating.

Based on the above analyses and experiments, although microcracks were found on the coating surfaces, it can be obviously concluded that there is an increasing accumulation of an apatite-like layer and enhancement in biomineralization of the composite ceramic coating with an increasing immersion time and content of TCP. In terms to reduce the microcracks after increasing the content of TCP, parameters optimization is necessary in the future work.

## 4. Conclusions

In this study, three different lasers (Nd:YAG pulsed laser, $CO_2$ CW laser, and Semiconductor laser) were used to successfully fabricate composite ceramic coatings on titanium alloy. Microstructures, mechanical performance, and bioactivity of the coatings were characterized. The key results are shown as follows:

(1) All these three kinds of lasers have successfully fabricated uniformly distributed Si3N4/TCP coatings. Besides, coatings fabricated by semiconductor laser showed the best surface morphologies.
(2) The microhardness of the TC4 sample could be greatly improved by the composite ceramic coating.
(3) The pure $Si_3N_4$ coating showed a lower apatite-like composition forming ability than the $Si_3N_4$/TCP samples in SBF, and there is an enhancement in biomineralization of the composite ceramic coating with an increasing immersion time and content of TCP.
(4) The work demonstrated the successful application of laser cladding for fabricating $Si_3N_4$/TCP composite ceramic coatings on biomedical Ti alloys.

## References


1. B.V. Krishna, S. Bose, and A. Bandyopadhyay, Low Stiffness Porous Ti Structures for Load-Bearing Implants, *Acta Biomater.*, 2007, **3**(6), p 997–1006
2. D. Kuroda, M. Niinomi, M. Morinaga, Y. Kato, and T. Yashiro, Design and Mechanical Properties of New i Type Titanium Alloys for Implant Materials, *Mater. Sci. Eng. A*, 1998, **243**(1), p 244–249
3. J.H. Ouyang et al., Characterization of Laser Clad Yttria Partially-Stabilized $ZrO_2$ Ceramic Layers on Steel 16MnCr5, *Surf. Coat. Technol.*, 2001, **137**(1), p 12–20
4. I.R. Pashby, S. Barnes, and B.G. Bryden, Surface Hardening of Steel Using a High Power Diode Laser, *J. Mater. Process. Technol.*, 2003, **139**(1-3), p 585–588
5. A. Bandyopadhyay et al., Influence of Porosity on Mechanical Properties and In Vivo Response of Ti6Al4V Implants, *Acta Biomater.*, 2010, **6**(4), p 1640–1648
6. V.K. Balla et al., Direct Laser Processing of a Tantalum Coating on Titanium for Bone Replacement Structures, *Acta Biomater.*, 2010, **6**(6), p 2329–2334
7. D.K. Pattanayak et al., Bioactive Ti Metal Analogous to Human Cancellous Bone: Fabrication by Selective Laser Melting and Chemical Treatments, *Acta Biomater.*, 2011, **7**(3), p 1398–1406
8. P. Lipinski, A. Barbas, and A.S. Bonnet, Fatigue Behavior of Thin-Walled Grade 2 Titanium Samples Processed by Selective Laser Melting. Application to Life Prediction of Porous Titanium Implants, *J. Mech. Behav. Biomed. Mater.*, 2013, **28**, p 274–290
9. J. Sun, Y. Yang, and D. Wang, Mechanical Properties of a Ti6Al4V Porous Structure Produced by Selective Laser Melting, *Mater. Des.*, 2013, **49**, p 545–552
10. F. Weng, C. Chen, and H. Yu, Research Status of Laser Cladding on Titanium and its Alloys: A Review, *Mater. Des.*, 2014, **58**, p 412–425
11. G.P. Dinda, J. Shin, and J. Mazumder, Pulsed Laser Deposition of Hydroxyapatite Thin Films on Ti-6Al-4V: Effect of Heat Treatment on Structure and Properties, *Acta Biomater.*, 2009, **5**(5), p 1821–1830
12. 侧向送丝激光熔覆成型技术的工艺研究及其数值模拟_孙进
13. L. Li, The Advances and Characteristics of High-Power Diode Laser Materials Processing, *Optics Lasers Eng*, 2000, **34**(4), p 231–253
14. Z. Shi et al., Silicon Nitride Films for the Protective Functional Coating: Blood Compatibility and Biomechanical Property Study, *J. Mech. Behav. Biomed. Mater.*, 2012, **16**, p 9–20
15. B.S. Bal and M.N. Rahaman, Orthopedic Applications of Silicon Nitride Ceramics, *Acta Biomater.*, 2012, **8**(8), p 2889–2898
16. T.J. Webster et al., Anti-Infective and Osteointegration Properties of Silicon Nitride, Poly(Ether Ether Ketone), Titanium Implants, *Acta Biomater.*, 2012, **8**(12), p 4447–4454
17. M. Mazzocchi and A. Bellosi, On the Possibility of Silicon Nitride as a Ceramic for Structural Orthopaedic Implants. Part I: Processing, Microstructure, Mechanical Properties, Cytotoxicity, *J. Mater. Sci.*, 2008, **19**(8), p 2881–2887
18. R.A. Surmenev, M.A. Surmeneva, and A.A. Ivanova, Significance of Calcium Phosphate Coatings for the Enhancement of New Bone Osteogenesis—A Review, *Acta Biomater.*, 2014, **10**(2), p 557–579
19. M. Roy et al., Laser Processing of Bioactive Tricalcium Phosphate Coating on Titanium for Load-Bearing Implants, *Acta Biomater.*, 2008, **4**(2), p 324–333
20. J.J. Candel and V. Amigó, Recent Advances in Laser Surface Treatment of Titanium Alloys, *J. Laser Appl.*, 2011, **23**(2), p 022005
21. H.M. Wang and Y.F. Liu, Microstructure and Wear Resistance of Laser Clad $Ti5Si_3$/$NiTi_2$ Intermetallic Composite Coating on Titanium Alloy, *Mater. Sci. Eng., A*, 2002, **338**(1-2), p 126–132
22. T. Kokubo and H. Takadama, How useful is SBF in predicting in vivo bone bioactivity? *Biomaterials*, 2006, **27**(15), p 2907–2915
23. J.L. Murray, *Binary Alloy Phase Diagrams*, ASM International, Materials Park, 1987
24. K. Kieswetter, Z. Schwartz, D.D. Dean, and B.D. Boyan, The Role of Implant Surface Characteristics in the Healing of Bone, *Crit. Rev. Oral Biol. Med.*, 1996, **7**, p 329–345